Hierarchical multi-phase microstructural architecture for exceptional strength-ductility combination in a complex concentrated alloy via high-temperature severe plastic deformation

Mageshwari Komarasamy[a], Tianhao Wang[a], Kaimiao Liu[a], Luis Reza-Nieto[a], and Rajiv S. Mishra[a,b,*]

[a]Center for Friction Stir Processing, Department of Materials Science and Engineering, University of North Texas, Denton, TX 76203, USA

[b]Advanced Materials and Manufacturing Processes Institute, University of North Texas, Denton, TX 76203, USA

*Corresponding author: email ID — Rajiv.Mishra@unt.edu

Abstract

Modification of a coarse B2 phase and realization of hierarchical multi-phase microstructures were achieved in an $Al_{0.5}CrFeCoNi$ complex concentrated alloy (CCA) using high-temperature severe plastic deformation (HTSPD). Under HTSPD conditions, a thermodynamically stable B2 phase dissolved, while a thermodynamically unstable coarse Al_3Ni phase formed. Al supersaturation in the matrix after HTSPD led to the formation of fine B2 precipitates during the subsequent aging treatment. The combination of Al_3Ni for enhanced work hardening and fine B2 precipitates for strength resulted in excellent strength-ductility of 1400 MPa and 20%.

Key words: $Al_{0.5}CrFeNiCo$; friction stir processing; Al_3Ni; strength; ductility

Modifying microstructures to achieve enhanced structural performance has always been key to satisfying various technological demands of recent centuries. This holds true even with new alloys such as complex concentrated alloys (CCAs) in which the compositional space has shifted from the edges of phase diagram to the center. CCAs consist of three or more principal elements either in equi- or non-equiatomic compositions, also encompasses high-entropy alloys (HEAs) that consist of five or more elements in equi- or non-equiatomic compositions [1,2]. CCAs exhibit excellent mechanical properties, thermal stability, and corrosion and wear resistance [3]. In addition to the initial effort of attaining only single-phase solid solutions (either face-centered

cubic, FCC or body-centered cubic, BCC), research is now focused on precipitation-hardened CCAs [4] and on dual-phase CCAs [5,6]. In compositions with FCC and NiAl-rich B2 phases, the cast structure consists generally of coarse B2, which deteriorates formability and damage tolerance. In general, thermomechanical processing is used to break and refine the coarse second phases. Refining the structure increases strength, but almost always reduces work hardenability due to the structure's reduced dislocation storage capability. Therefore, designing alloys and thermomechanical processing and heat treatment steps to improve both strength and ductility is imperative.

In a previous work, Al powders were added to $Al_{0.1}$CrFeCoNi CCA and then friction stir processed (FSPed) that created Al-rich regions consisting of B2 and Al_3Ni phases that increased both strength and ductility [7]. Friction stir processing (FSP) is a high-temperature severe plastic deformation (HTSPD) technique that is capable of deforming and eventually dissolving second phases (miscible or even immiscible with the matrix) [8]. In the current investigation, FSP-based HTSPD was used to tailor the microstructure of $Al_{0.5}$CrFeCoNi CCA with FCC and coarse B2 phases. A coarse second phase that promote work hardenability is expected after HTSPD (based on previous investigation [7]) while fine strengthening phase is expected after aging due to solute supersaturation that overall would lead to a good strength-ductility combination. Detailed microstructural evolution through microscopy, X-ray diffraction analyses and the corresponding phase formation mechanisms, as well as a complete mechanical property evaluation, were carried out.

The elemental mixture required to fabricate $Al_{0.5}$CrFeCoNi CCA was vacuum induction melted, cast into a 2″ × 6 ″ × 15 ″ ingot that was then hot-rolled to 1″ at 1150ºC, and subsequently water-quenched. FSP-based HTSPD was performed using a W-Re tool of 12 mm shoulder diameter

and 3.5 mm pin length. Following HTSPD processing parameters were used: tool rotation rate of 600 revolutions per minute and traverse speed of 2 inches per minute. In the HTSPD condition, samples for aging heat treatment and tensile testing were cut. Aging heat treatments were done at 550ºC, 630ºC, 700ºC, 850ºC, and 1100ºC for varying times. All samples for both hardness and tensile tests were polished to 1 µm surface finish, while all microscopy samples were polished to 0.02 µm surface finish. Hardness measurements were done with a Vickers microhardness tester at 200 g load with dwell time of 10 seconds. Based on aging curves, 700ºC for 6 hours (HT) was selected for tensile testing in addition to cast + hot-rolled and HTSPD conditions. Tensile sample dimensions were 2 mm gage length, 1 mm width, and ~0.7 mm thickness. All tensile tests were done with a custom-built tensile testing machine operated at an initial strain rate of 1×10^{-3} s^{-1}. Both electron backscattered diffraction (EBSD) and scanning electron microscopy (SEM) in backscattered electron (BSE) mode were done for cast + hot-rolled, HTSPD, and HTSPD + HT in FEI Nova NanoSEM 230 with Hikari Super EBSD. FEI Quanta 200 was used for energy dispersive spectroscopy (EDS) analysis. Rigaku III Ultima X-ray diffractometer was used for X-ray diffraction (XRD) analysis. Post-deformation analysis of the fractured HTSPD sample using EBSD was carried out.

Chemical composition of the cast + hot-rolled material was 10.56Al-22.21Cr-22.51Fe-22.47Co-22.25Ni (in at. %), which is close to the nominal composition of 11.11Al-22.22 Cr-22.22Fe-22.22Co-22.22Ni (in at. %). The microstructure of the cast + hot-rolled condition is given in Figures 1 (a)–(c). Coarse and fine B2 phases are denoted by magenta and green arrows, respectively. Image quality (IQ) + phase map obtained from EBSD analysis also shows coarse and fine B2 (green) in the FCC matrix (red) (Figure 1 (c). Easy crack initiation and propagation are expected due to coarse B2 in the cast condition, which was reflected in poor tensile

deformation behavior that is discussed later. Therefore, this microstructure was subjected to intense HTSPD to modify the size and distribution of the microstructural features to introduce hierarchically evolved structures for both high strength and ductility. BSE-SEM and EBSD images of the microstructural evolution after HTSPD (Figures 1 (d)–(f)) confirm the absence of fine B2 and a significantly reduced fraction of coarse B2, as noted distinctly and as based on the evidence in Figures 1 (a) and (d) which, by the way, are of the same magnification. A similar observation is also revealed in the EBSD analysis (Figure 1 (f)). In addition to that, fine particles exhibiting darker contrast in BSE-SEM mode are denoted by white arrows (Figures 1 (d and e)). Discussion on the nature of these second phases follows.

FSP-based HTSPD involves high strain rate, high temperature (0.5-0.9Tm), and severe plastic strain [9]. During HTSPD, the material undergoes extreme conditions of deformation; the expected pathway of the microstructural evolution is presented in supplementary Figure 1. Both FCC and B2 (fine and coarse) undergo severe plastic deformation at high temperature that elongated and eventually fractured B2 phases into a finer structure. With continued deformation, all of the fine B2 and most of the coarse B2 dissolved into the FCC matrix. At this point during HTSPD, due to B2 dissolution, the Al content in the FCC matrix exceeds the solubility limit, which leads to the formation of second phases (denoted by white arrows in Figures 1 (e)). The region with and without second phases exhibited fine and coarse grain sizes, respectively (Figures 1 (e) and (f)). As expected, second-phase particles limited grain growth due to the ‘Zener pinning’ effect. However, due to the limitation on time, the second-phase fraction from dynamic precipitation would be limited, thus leaving a large fraction of Al in the FCC matrix for further precipitation. Also note that the region surrounding the undissolved B2 did not have the second phases.

EDS spot analysis of both FCC and B2 phases of the cast + hot-rolled material and the regions with and without second phases are given in Table 1. Composition of the B2 phase was enriched in Al and Ni, while Al was depleted in the FCC phase. Furthermore, Al fraction in the HTSPD processed volume is significantly larger than the Al fraction in the FCC phase in the cast + hot-rolled condition. The overall evolved microstructure would contain an Al-enriched FCC phase; remnant, deformed, and fractured B2 phases; and the newly-formed phases.

XRD analysis of cast + rolled, HTSPD, and HTSPD + HT is shown in Figure 2 (a) as Figures (a_1), (a_2), and (a_3), respectively. In all three conditions, both FCC and B2 phases were present. Interestingly, in the HTSPD condition, peaks corresponding to the Al_3Ni phase ($D0_{11}$) were evident. The inset in Figure (a_2) shows the multiple peaks corresponding to the Al_3Ni phase obtained from a fine XRD scan with small step size. In the HTSPD condition, dissolution of the B2 phase led to reduced relative peak intensity of B2 to FCC as compared with the two other conditions. Furthermore, Al_3Ni peaks remained after aging treatment at 700ºC for 6 hours. A pseudo-binary phase diagram of $CrFeCoNiAl_{x\ (x=0\ to\ 1)}$ using PANDAT HEA database is presented in Figure 2 (b). The blue line represents alloy composition. The expected phases are FCC, B2, Sigma, and $L1_2$. All experimental evidences so far on Al-containing CCAs, especially in Al $\geq$ 0.3 mole fraction, include B2 (NiAl-based) intermetallics, and none of the reports featured Al_3Ni or any Al-rich intermetallic phase. Figure 2 (c) shows the Gibbs free energy and effective heat of formation for all major phases in the Al-Ni binary system. Information on the effective heat of formation calculation is taken from [10]. In the Al-lean region, the stable phases are Ni_3Al and NiAl; while Al_3Ni_2 and Al_3Ni are stable only in the Al-rich region. The red line represents the Al to Ni ratio based on $Al_{0.5}CrFeCoNi$, which is 1:2 or 33.33% of Al and 66.67% of Ni and falls on the Al-lean region.

During HTSPD of high-temperature materials, the expected processing temperature is ~ 900–1100ºC [11]. In the case of the Al-Ni binary system, depending on composition, Al_3Ni forms in liquid Al from 640–850ºC. Therefore, based on Gibbs free energy analysis for binary Al-Ni, Al_3Ni should not be stable above 850ºC. As stated above [7], pure Al powders were added to $Al_{0.1}$CrFeCoNi CCA, which was then processed by FSP. The high temperature during processing caused the Al powder to melt first, such that the resultant local enrichment in Al concentration promoted the formation of the Al_3Ni phase [7]. In the current study, no such enrichment in composition was possible, as was also confirmed by spot EDS analysis. Overall, based on both theoretical and experimental evidences, an Al_3Ni phase should not form in $Al_{0.5}$CrFeCoNi CCA during HTSPD.

Among all Al-Ni based intermetallic phases, Al_3Ni exhibits the highest heat of formation value; while AlNi registers the lowest heat of formation thus making it a more stable phase. In the case of Al/Ni multilayers prepared by repeated folding and cold-rolling, severe plastic deformation resulted in the interface being supersaturated with solid solutions with varying Al and Ni fractions [11]. And subsequent annealing treatments resulted in the formation of Al_3Ni at different locations irrespective of the varying Al and Ni fractions [12]. Therefore, the necessary conditions are severe plastic deformation and the associated point and line defects concentration in high density that accelerates the formation of an orthorhombic phase in an FCC matrix. The extent of plastic strain can be noted from the almost complete dissolution of the B2 phase. Therefore, based on chemical-free energy, AlNi should be the stable phase; however, the increased contribution from defect-based free energy counteracted the chemical contribution and led to the formation of Al_3Ni. A detailed explanation for Al_3Ni formation is not understood and

is outside the scope of this work. Nevertheless, the manifestation of the coarse Al_3Ni phase is paramount to achieving a good combination of strength-ductility, and is discussed later.

HTSPD was performed to break and dissolve the coarse B2 phase thereby led to Al-enrichment in the FCC matrix. Therefore, controlled aging treatments will precipitate out fine second phase precipitates. Aging conditions were chosen based on the pseudo-binary phase diagram (Figure 2 (b)); horizontal lines indicate various aging heat treatments. The Table in Figure 3 (a) shows a list of expected phases. B2 precipitation is expected for all heat treatment conditions except for 550ºC, where Ni_3Al ($L1_2$-type) precipitates. Results of aging treatments are compared with cast + hot-rolled and HTSPD conditions and are given in Figure 3 (a). Among all the conditions, HTSPD + HT exhibited the highest hardness. Interestingly, B2 (NiAl-based) precipitates are effective strengtheners as compared to $L1_2$ (Ni_3Al). As expected, 1100ºC exhibited the lowest hardness among the aging conditions due to coarse B2 precipitates (SEM image is not included here). Figures 3 (b), (c) show the microstructure for the HT condition. The finer in-grain precipitates are the B2 precipitates (red arrows), which are uniform throughout the HTSPD processed volume. The high magnification image clearly reveals the needle-shaped morphology of B2 precipitates (Figure 3 (c)). Thickness of the fine B2 ranged from ~10 to 50 nm, and length of the precipitates was below 1 µm, with a few exceptions of more than a few µm long precipitates. Exceptional hardness of the HTSPD + optimized aging heat treatment is due mainly to the fine B2 precipitates. The precipitates marked with white arrows are the Al_3Ni phase.

Tensile properties of various microstructural states are presented in Figure 4 (a). In the cast + hot-rolled condition, due to coarse B2 that aided in easy crack nucleation and propagation, tensile ductility was the lowest, while both processed conditions exhibited multiple fold increase in ductility regardless of high strength. For instance, yield strength varied from 681 MPa in cast

+ hot-rolled condition to 772, and 1133 MPa in HTSPD and HTSPD + HT, respectively; while ductility increased significantly from 8.2% to 30.3% and 19.3%, respectively. Figure 4 (b) shows work hardening characteristics for the three conditions. Both HTSPD and HTSPD + HT conditions exhibited sustained work hardening during Stage B, while cast + hot-rolled exhibited limited work hardening. The origin of the work hardening can be discussed with the post-deformation EBSD analysis of Figure 4 (c) in the form of phase (Figure 4(c_1)) and Kernal average misorientation (KAM) maps (Figure 4 (c_2)). The region inside the dotted polygon had relatively fewer Al_3Ni precipitates as compared to the region outside of it. Interestingly, based on KAM analysis, regions with Al_3Ni precipitates exhibited large lattice misorientation, which indicates relatively high dislocation density as compared to the regions without the Al_3Ni phase. As mentioned earlier, regions with Al_3Ni exhibited finer grains as compared to regions without, and extensive deformation in coarse grains rather than in fine grains is expected. This, however, was not the case. Additionally, CrFeCoNi-based CCAs exhibit low SFE [13] that would eventually lead to the formation of deformation twins. The composition of regions with and without the Al_3Ni phase was similar and would lead to the same extent of deformation twinning; hence, to similar lattice misorientation values. However, an explicit difference in KAM values between Al_3Ni-rich and lean regions denoted the increased dislocation storage in the Al_3Ni-rich regions that contributed to sustained work hardening in the HTSPD conditions in addition to the deformation twinning contributions. A comparison of the current results with various alloys is presented in Figure 4 (d). The HTSPD + HT condition exhibited the best combination of strength and ductility among all the alloys listed. Clearly, the combination of hierarchical microstructural features, i.e., thin B2 precipitates for strength and coarse Al_3Ni for enhanced work hardening, led to strength of 1400 MPa with 20% fracture elongation.

The microstructure of $Al_{0.5}CrFeCoNi$ CCA with coarse B2 phase was modified via HTSPD and subsequent aging to attain an excellent combination of strength and ductility. Following are the major conclusions:

1. The thermodynamically stable B2 phase was dissolved, whereas a thermodynamically unfavorable Al_3Ni phase was formed during FSP-based HTSPD. Extensive defects in the HTSPD processed volume are likely to account for the formation of Al_3Ni.
2. Due to the dissolution of the B2 phase during HTSPD, Al was enriched in the FCC matrix. The enriched matrix was used to precipitate out fine B2 precipitates in subsequent aging heat treatment.
3. With the combination of fine B2 precipitates for strength and Al_3Ni for ductility, the alloy after HTSPD + HT exhibited UTS of 1400 MPa and fracture elongation of 20%.

Acknowledgments

The work was performed under a cooperative agreement between the Army Research Laboratory and the University of North Texas (W911NF-16-2-0189). Authors acknowledge Materials Research Facility (MRF) for all the microscopy facilities.

References

[1] J.W. Yeh, S.K. Chen, S.J. Lin, J.Y. Gan, T.S. Chin, T.T. Shun, C.H. Tsau, S.Y. Chang, Adv. Eng. Mater. 6 (2004) 299–303.

[2] B. Cantor, I.T.H. Chang, P. Knight, A.J.B. Vincent, Mater. Sci. Eng. A 375–377 (2004) 213–218.

[3] D.B. Miracle, O.N. Senkov, Acta Mater. 122 (2017) 448–511.

[4] J.Y. He, H. Wang, H.L. Huang, X.D. Xu, M.W. Chen, Y. Wu, X.J. Liu, T.G. Nieh, K. An, Z.P. Lu, Acta Mater. 102 (2016) 187–196.

[5] J.Y. He, W.H. Liu, H. Wang, Y. Wu, X.J. Liu, T.G. Nieh, Z.P. Lu, Acta Mater. 62 (2014) 105–113.

[6] Z. Li, K.G. Pradeep, Y. Deng, D. Raabe, C.C. Tasan, Nature 534 (2016) 227–230.

[7] T. Wang, S. Shukla, M. Komarasamy, K. Liu, R.S. Mishra, submitted to Materials Letters.

[8] K. Mageshwari, R.S. Mishra, S. Mukherjee, M.L. Young, Jom 67 (2015) 2820–2827.

[9] R.S. Mishra, P.S. De, N. Kumar, Friction Stir Welding and Processing, Springer International Publishing, Cham, 2014.

[10] D. Shi, B. Wen, R. Melnik, S. Yao, T. Li, J. Solid State Chem. 182 (2009) 2664–2669.

[11] V. Tungala, A. Arora, B. Gwalani, R.S. Mishra, R.E. Brennan, K.C. Cho, Mater. Sci. Eng. A 709 (2018) 105–114.

[12] X. Sauvage, G.P. Dinda, G. Wilde, Scr. Mater. 56 (2007) 181–184.

[13] S.F. Liu, Y. Wu, H.T. Wang, J.Y. He, J.B. Liu, C.X. Chen, X.J. Liu, H. Wang, Z.P. Lu, Intermetallics 93 (2018) 269–273.

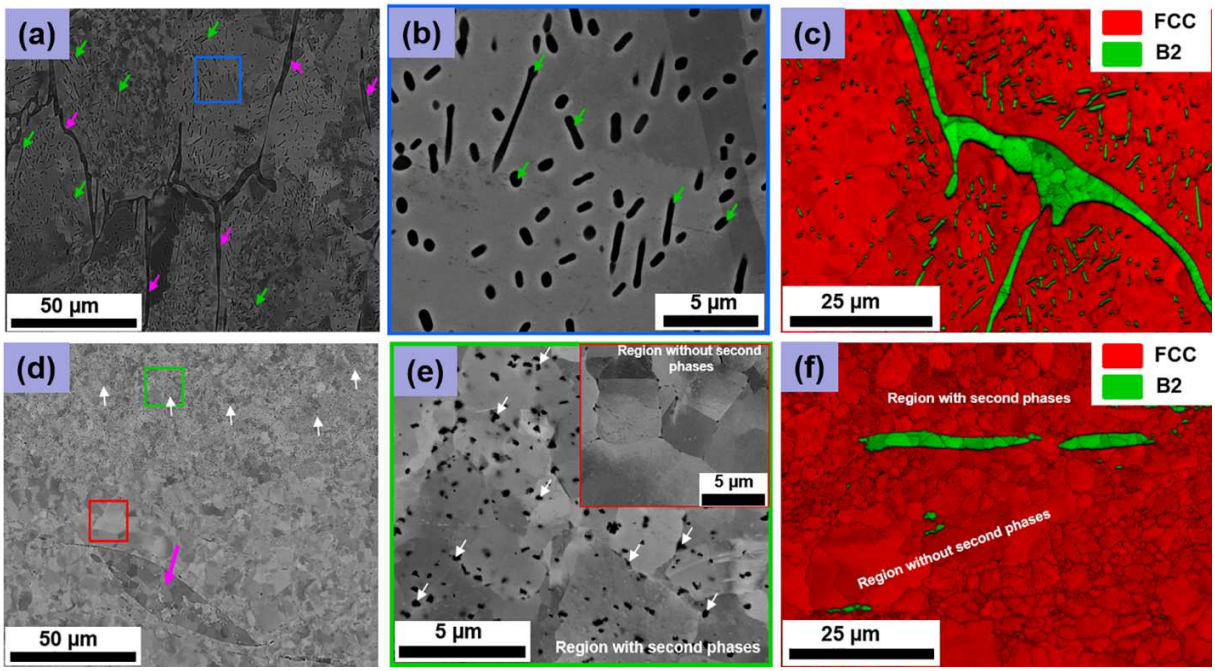

Figure 1. (a)–(c) Microstructural analysis of cast + hot-rolled condition. (a), (b) Low and high magnification BSE-SEM images showing coarse (magenta arrows) and fine (green arrows) B2 phases, respectively. (c) EBSD IQ + phase map showing both FCC and B2 phases. (d)–(f) Microstructural analysis of HTSPD condition. (d) Low magnification image of the remnant B2 phase and fine particles marked by white arrows, (e) high magnification images of the regions marked by green and red boxes in (d) showing regions with and without second phases, and (f) IQ + phase map showing the phase distribution after HTSPD.

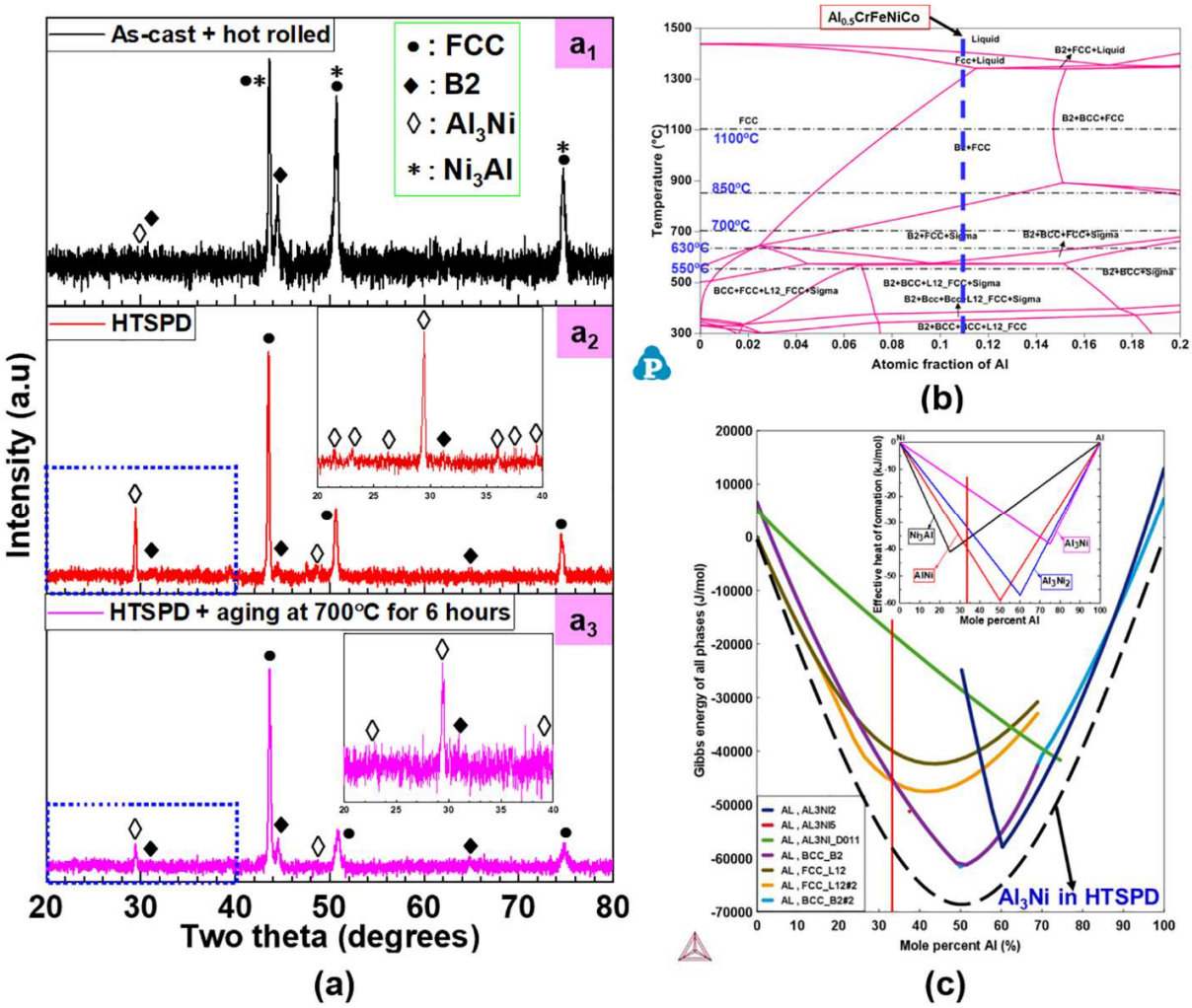

Figure 2. (a) XRD analysis of cast + hot-rolled, HTSPD, and HTSPD + HT are presented in (a_1), (a_2), (a_3), respectively, (b) pseudo-binary phase diagram for $CrFeCoNiAl_{x(0:1)}$, and (c) Gibbs free energy and an inset showing effective heat of formation for all phases as functions of mole percent of Al.

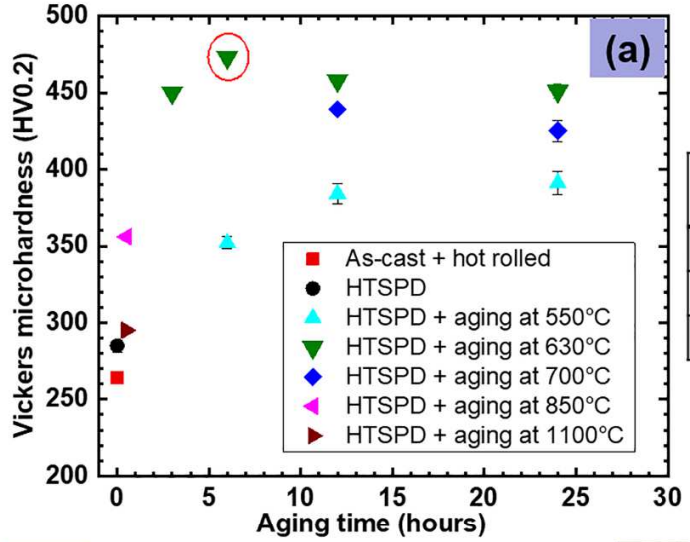

Aging temperature (°C)	Equilibrium phases
550	$L1_2$
630 and 700	B2 and Sigma
850 and 1100	B2

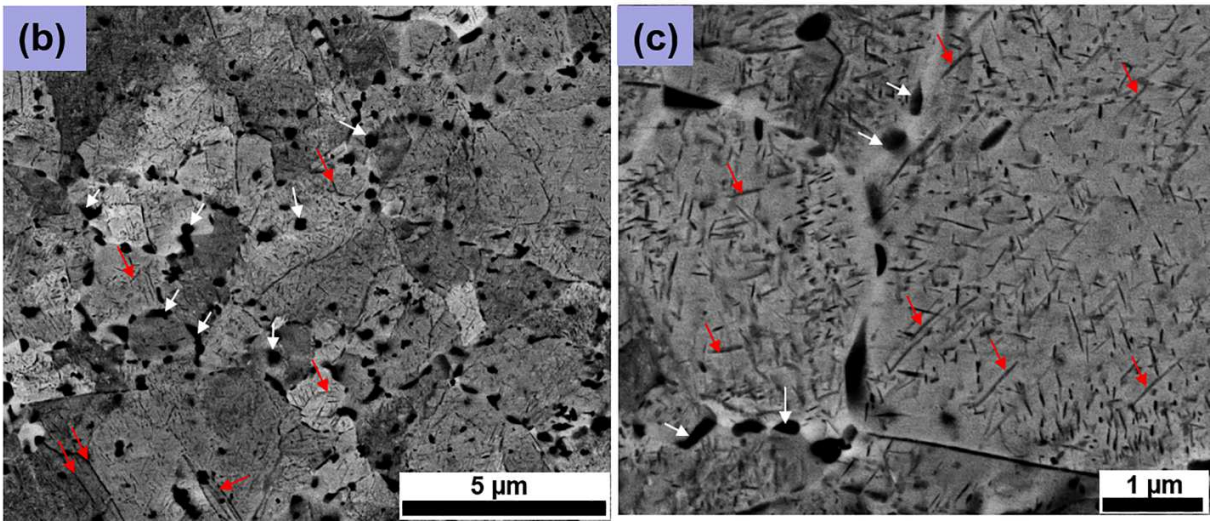

Figure 3. (a) Age hardening curves for various aging time with expected equilibrium phases listed on the right, and (b) low and (c) high magnification images showing B2 precipitates.

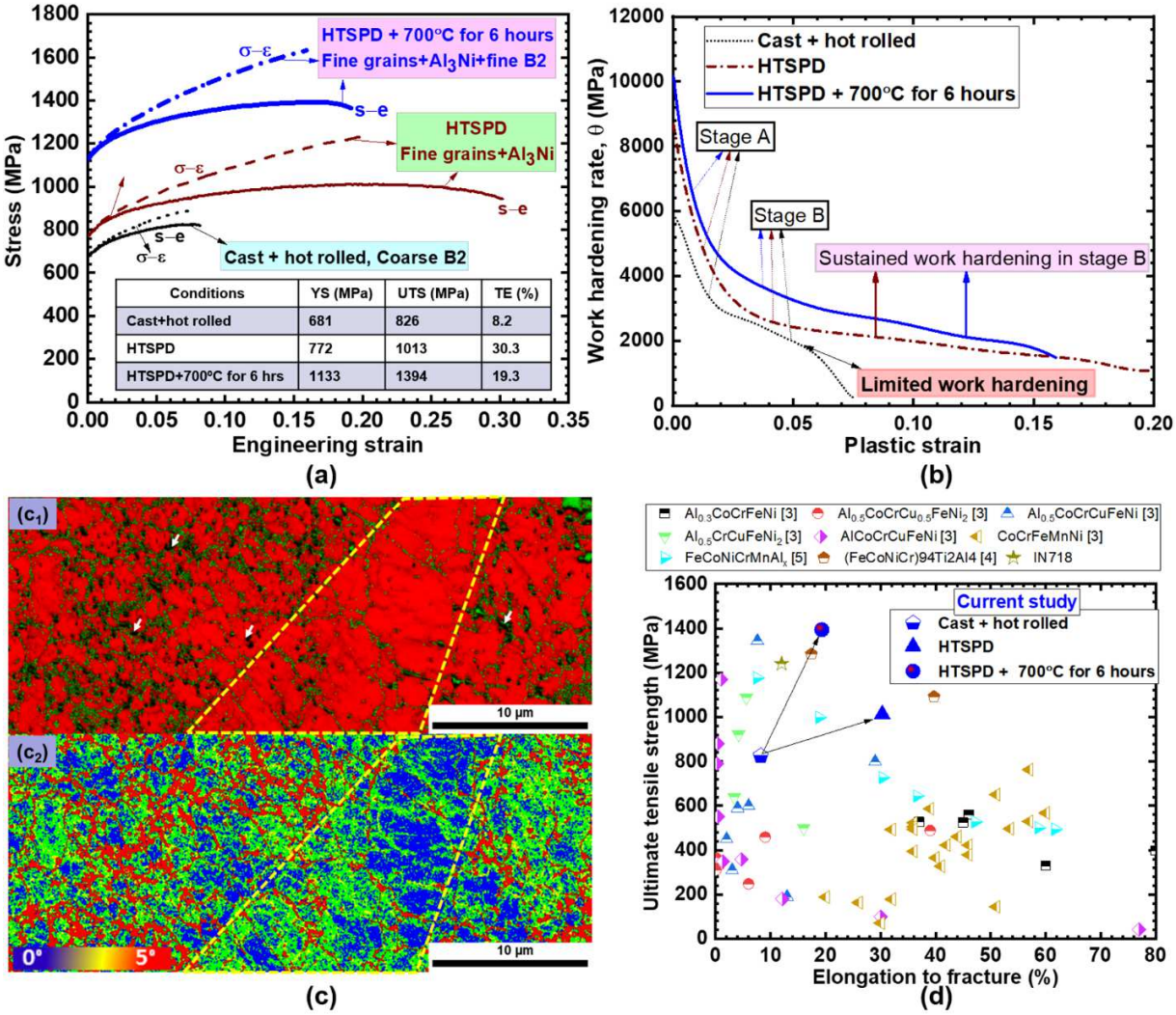

Conditions	YS (MPa)	UTS (MPa)	TE (%)
Cast+hot rolled	681	826	8.2
HTSPD	772	1013	30.3
HTSPD+700°C for 6 hrs	1133	1394	19.3

Figure 4. (a) Engineering and true stress-strain curves for all conditions with an inset table that summarizes tensile properties, (b) work hardening rate curves, and (c) post-deformation EBSD analysis showing phase and KAM maps. A low magnification post-deformation EBSD analysis is presented in supplementary Figure S2. (d) Comparison of the current tensile properties with various CCAs and a superalloy IN718.

Table 1. EDS spot analysis of both cast + hot rolled and HTSPD conditions (in at. %)

	Cast+hot-rolled		**HTSPD**	
	FCC	**B2**	**Spots on the region without second phase**	**Spots on the region with second phase**
Al	8.35±0.24	27.59±3.35	9.97±0.17	10.41±0.31
Cr	23.34±0.33	9.56±2.20	22.53±0.15	22.27±0.17
Fe	23.79±0.23	12.72±1.73	23.04±0.17	22.74±0.17
Co	23.43±0.09	17.52±1.09	22.96±0.14	22.83±0.11
Ni	21.04±0.40	32.60±1.68	21.51±0.28	21.75±0.15

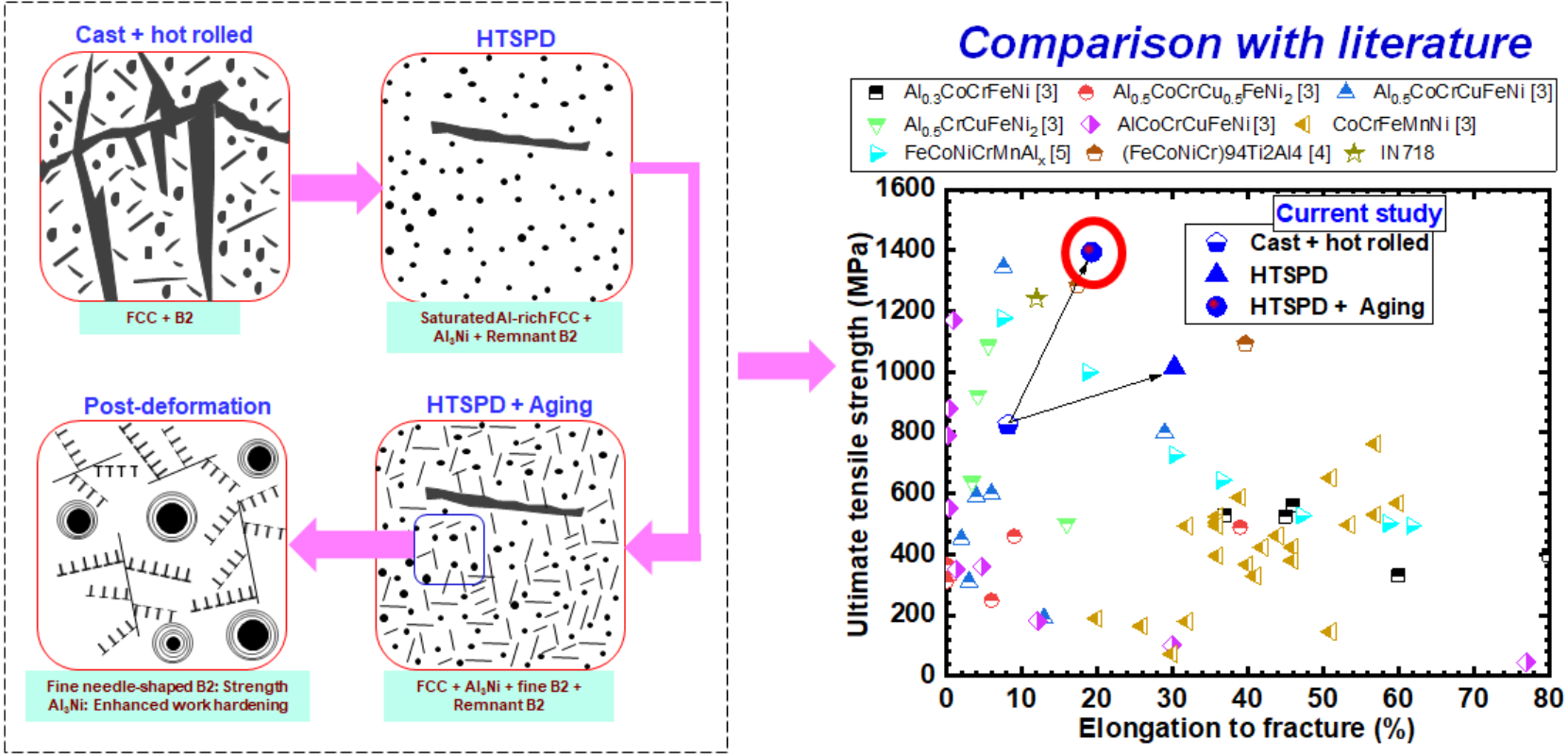
Cast + hot rolled
FCC + B2
HTSPD
Saturated Al-rich FCC + Al3Ni + Remnant B2
HTSPD + Aging
FCC + Al3Ni + fine B2 + Remnant B2
Post-deformation
Fine needle-shaped B2: Strength
Al3Ni: Enhanced work hardening
Comparison with literature
Al0.3CoCrFeNi [3]
Al0.5CoCrCu0.5FeNi2 [3]
Al0.5CoCrCuFeNi [3]
Al0.5CrCuFeNi2 [3]
AlCoCrCuFeNi [3]
CoCrFeMnNi [3]
FeCoNiCrMnAlx [5]
(FeCoNiCr)94Ti2Al4 [4]
IN718
Current study
Cast + hot rolled
HTSPD
HTSPD + Aging
Ultimate tensile strength (MPa)
Elongation to fracture (%)
0
200
400
600
800
1000
1200
1400
1600
0
10
20
30
40
50
60
70
80